JOURNAL OF SOLID STATE CHEMISTRY 30, 171–181 (1979)

Magnetic and Spectroscopic Investigation of Partially Reduced Vanadium Pentoxides. III. $(Mo_xV_{1-x})_2O_5$*

F. Y. ROBB AND W. S. GLAUNSINGER†
Department of Chemistry, Arizona State University, Tempe, Arizona 85281

AND P. COURTINE

Département de Genie Chimique, Université de Technologie de Compiegne, Compiegne, 60206, France

Received June 28, 1978; in revised form November 3, 1978.

The magnetic, electron paramagnetic resonance (EPR), infrared (ir), and optical properties of the orthorhombic ($x \leq 0.20$) and monoclinic ($x = 0.28$) phases of $(Mo_xV_{1-x})_2O_5$ have been measured and interpreted. The magnetic data are interpreted in terms of a ligand-field model in which the octahedral $^2T_{2g}$ term of V^{4+} is split by the combined perturbations of axial distortion and spin-orbit coupling, with the result that the $^2T_{2g}$ term is split into a magnetic ground level, a weakly magnetic intermediate level, and a magnetic highest level. The g-values and linewidth data are in good agreement with the magnetic results. The susceptibility and EPR studies indicate that the paramagnetic centers are deep-donor V^{4+}–O–Mo^{6+} pairs and that the oxygen symmetry is more nearly octahedral in the monoclinic phase. The ir spectra indicate a weakening of the shortest metal–oxygen bond in the monoclinic phase, and the optical spectra show a concomitant increase in the octahedral component of the ligand field in this phase. The implications of these results for oxidation catalysis by $(Mo_xV_{1-x})_2O_5$ are discussed.

Introduction

Mixed oxides are frequently used to catalyze oxidation reactions. In particular, catalysts composed of V_2O_5 and MoO_3, often containing small quantities of other oxides, are employed in the catalytic oxidation of several organic compounds, such as the oxidation of benzene to maleic anhydride (*1*). A few attempts have been made to correlate the physicochemical properties of the V_2O_5–MoO_3 system with its catalytic activity, which is optimal in the range 25–28 mole% MoO_3 (*1–8*). These studies have shown that within the range 25–33 mole% MoO_3 the V^{4+} concentration (*3, 4, 6*) and electrical conductivity are maximal and the activation energy is minimal (*5*) in these semiconductors. A shift in the infrared band near 1000 cm^{-1} due to multiple metal–oxygen bonds to lower frequencies with increasing Mo content has also been observed (*4, 7*).

The phase relations and crystal structures of the V_2O_5–MoO_3 oxides may provide important information for understanding their catalytic behavior. It has been shown that molybdenum can replace vanadium in V_2O_5 and that this replacement produces a solid solution of composition $(Mo_xV_{1-x})_2O_5$ extending at 650°C to $x = 0.28$ (*9*). However, a detailed structural examination reveals that the structure changes from orthorhombic to monoclinic near $x = 0.20$

* This research was supported in part by Grant DMR75-09215 from the National Science Foundation.

† To whom to address inquiries.

0022-4596/79/110171-11$02.00/0

(*9*). The structures of monoclinic $(Mo_{0.28}V_{0.72})_2O_5$ (*9*) and orthorhombic V_2O_5 (*10*) are shown in Fig. 1. The structures consist of edge-shared octahedra which form zigzag chains in the *c* direction, with these chains being connected by corner sharing between octahedra in adjacent chains. The structures can also be considered to consist of ReO_3-type slabs, with each slab being two octahedra thick, in the *bc* plane which are connected to adjacent slabs by edge sharing. The major difference between the two structures is the displacement of the metal ions from the centers of the octahedra. In the V_2O_5 structure all metal ions within an ReO_3-type slab are displaced in the same direction, whereas in the monoclinic structure they are shifted pairwise in opposite directions. In both structures the metal ions in edge-shared octahedra are displaced in opposite directions to minimize electrostatic repulsions. The metal–oxygen distances for both structures are given in Table I. The more nearly equal metal–oxygen distances in

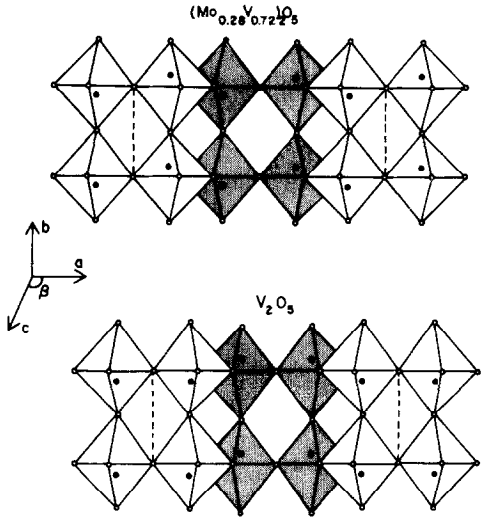

FIG. 1. The structures of $(Mo_{0.28}V_{0.72})_2O_5$ (top) and V_2O_5 (bottom) constructed from MO_6 octahedra at two levels. Shaded octahedra are situated at a lower level than the unshaded octahedra. The positions of the metal ions within the octahedra are indicated by dots. (Adapted from Ref. (*9*).)

TABLE I

METAL–OXYGEN DISTANCES IN $(Mo_{0.28}V_{0.72})_2O_5$ AND V_2O_5

Bond	$(Mo_{0.28}V_{0.72})_2O_5$ distances[a] (Å)	V_2O_5 distances[b] (Å)
M–O_1	1.659	1.585
M–O_2	1.733	1.780
M–O_3	1.804	1.878
M–O_4	2.081	1.878
M–O_5	2.094	2.021
M–O_6	2.544	2.785

[a] Reference (*9*).
[b] Reference (*10*).

$(Mo_{0.28}V_{0.72})_2O_5$ imply that the metal–oxygen polyhedra have a more pronounced octahedral arrangement in the monoclinic phase.

In this paper we have undertaken a comprehensive study of the magnetic, electron paramagnetic resonance (EPR), infrared (ir), and optical properties of the orthorhombic and monoclinic phases of $(Mo_xV_{1-x})_2O_5$ in an attempt to help understand the behavior of these interesting and useful catalysts by better defining their physicochemical properties.

Experimental

Samples were prepared by heating mixtures of V_2O_5, V_2O_3, and MoO_3 according to the equation:

$$2x\ MoO_3 + \frac{x}{2} V_2O_3 + \left(1 - \frac{3x}{2}\right) V_2O_5 \rightarrow (Mo_xV_{1-x})_2O_5. \quad (1)$$

The starting materials were Johnson–Matthey Specpure V_2O_5 and Mallinckrodt MoO_3, both of which contained negligible paramagnetic impurity concentrations. V_2O_3 was prepared by reduction of V_2O_5 with hydrogen at 800°C for 12 hr. The mixtures were contained in a sealed silica tube at

650°C. After a first firing for 48 hr, the tube was broken and the samples were reground and refired until thin X-ray powder patterns indicated that they were monophasic. In agreement with Kilborg (*9*), we have found that for $x \leq 0.20$ the unit cell is orthorhombic, and in the range $0.20 \leq x \leq 0.28$ it is monoclinic. For $x \geq 0.30$ a few weak lines could be assigned to $VOMoO_4$. The compositions $x = 0.10$, 0.25, and 0.28 were selected for detailed study, and their unit-cell dimensions, which are in reasonable agreement with previous studies (*9, 11*), are given in Table II.

The magnetic susceptibility was measured and corrected as described in II. MoO_3 exhibited a temperature-independent paramagnetism of 24×10^{-6} emu/mole in the range 1.5–300°K, so that, in view of this small susceptibility and the rather low Mo content of the samples, the susceptibilities were not corrected for the temperature-independent paramagnetism of MoO_3. EPR, ir, and optical spectra were also recorded as described in II.

Results and Discussion

Magnetic Susceptibility

The reciprocal susceptibility per mole of $(Mo_xV_{1-x})_2O_5$ as a function of temperature is shown in Fig. 2. The increase in susceptibility with Mo concentration above 100°K suggests a corresponding increase in paramagnetic ion concentration. The high-temperature data can be fitted to the Curie–Weiss law, $\chi = C/(T-\theta)$, where C and θ are the Curie and Weiss constants, respectively. The magnetic moment per mole of Mo is given by $\mu = 2.828\ (C/2x)^{1/2}$. The magnetic parameters C, θ, and μ for $(Mo_xV_{1-x})_2O_5$ are given in Table III.

The magnetic moments are nearly independent of molybdenum concentration and close to the spin-only value, which indicates that the substitution of molybdenum for vanadium is accomplished by the formation of a paramagnetic center having one unpaired electron, most likely $Mo^{5+}(4d')$ or $V^{4+}(3d')$. That the paramagnetic ion is indeed V^{4+} has been shown by its characteristic hyperfine structure in samples with low Mo content (*2*) and is also indicated by the magnetic analysis given below and by the EPR results discussed in the next section.

Since there is no evidence for magnetic ordering down to 2°K, θ is not significant as an interaction constant, and, as in II, it is possible to interpret the magnetic behavior in terms of the effective magnetic moment $\mu_{eff} = 2.828\ (\chi T)^{1/2}$. Theoretical expressions from which μ_{eff} can be calculated for a d' ion in an octahedral ligand field under the combined perturbations of axial distortion and spin–orbit coupling have been given in I. In $(Mo_xV_{1-x})_2O_5$ the axial distortion occurs along the shortest $V^{4+}-O$ bonds and relative to this direction the oxygen symmetry is approximately C_{4v}. The ligand-field parameters for $(Mo_xV_{1-x})_2O_5$ obtained by a least-squares fit of the theoretical moments to the experimental ones are given in Table IV. Figures 3 and 4 show the agreement

TABLE II

UNIT-CELL DIMENSIONS OF $(Mo_xV_{1-x})_2O_5$

x	a (Å)	b (Å)	c (Å)	β (deg)
0.00	11.50	4.37	3.56	90.0
0.10	11.57	4.32	3.59	90.0
0.25	11.80	4.18	3.64	90.6
0.28	11.81	4.17	3.65	90.6

TABLE III

MAGNETIC PARAMETERS FOR $(Mo_xV_{1-x})_2O_5$

x	C (emu · deg · mole^{-1})	θ (°K)	μ/β (g-atom Mo^{-1})
0.10	0.078	−38	1.77
0.24	0.182	−60	1.71
0.28	0.222	−93	1.78

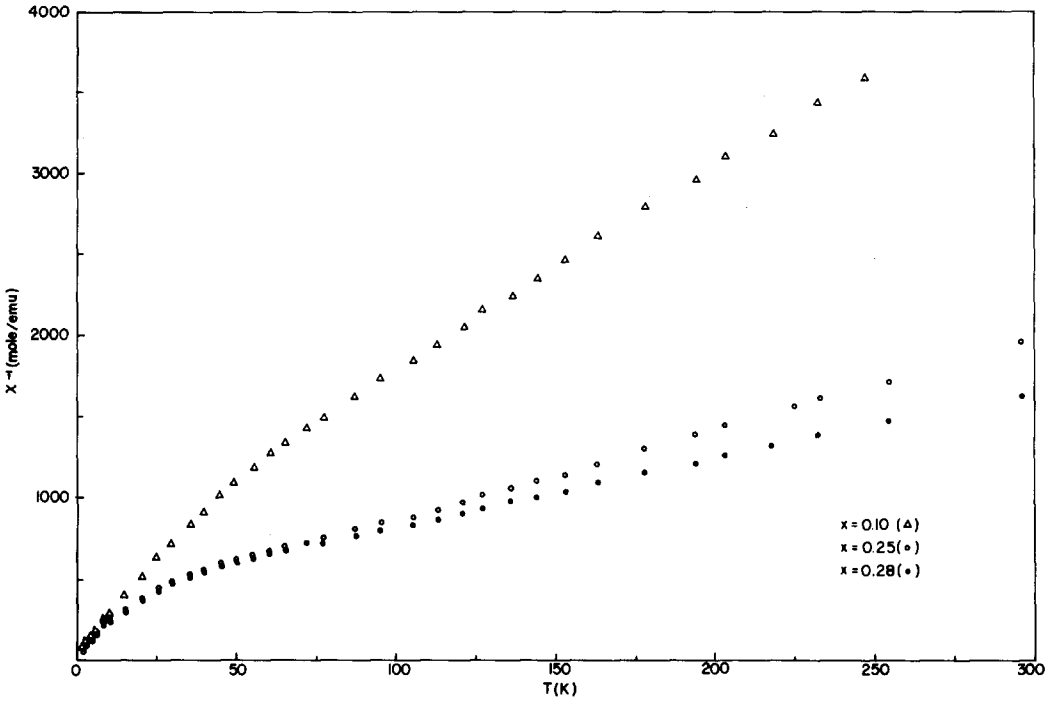

FIG. 2. Temperature dependence of the reciprocal molar susceptibility of $(Mo_xV_{1-x})_2O_5$.

between the theoretical and experimental moments and the corresponding energy-level diagram for $(Mo_{0.28}V_{0.72})_2O_5$. As found in I and II, the ordering of the energy levels is $\Gamma_7(B)<\Gamma_6(E)<\Gamma_7(E)$, so that V^{4+} has a magnetic ground level, a weakly magnetic intermediate level, and a magnetic highest level.

The parameters k, λ, and Δ in Table III can be interpreted in terms of the electronic and crystal structure of $(Mo_xV_{1-x})_2O_5$. The value $k = 1$ at $x = 0.10$ indicates that the $3d'$ electron is localized on V^{4+}, and the value $k = 0.8$ for $x = 0.25$ and 0.28 reflects a partial delocalization of the paramagnetic electron onto the surrounding ligands. However, the k values and activation energies (≥ 0.67 eV for $x \leq 0.33$) (*5*) are considerably higher than in β'-$Cu_xV_2O_5$ (*12*) for a given V^{4+} concentration. The relatively high k values and activation energies and nearly spin-only magnetic moments in $(Mo_xV_{1-x})_2O_5$ can be accounted for by assuming that the substitution of Mo^{6+} for V^{5+} in these solids results in the formation of V^{4+}–O–Mo^{6+} pairs, which act as deep donors because the paramagnetic electron is effectively trapped by its electrostatic attraction to Mo^{6+}. This deep-donor center has also been suggested in the system $Na_xV_{2-x}Mo_xO_5$ on the basis of atomic distributions (*13*). In $(Mo_xV_{1-x})_2O_5$ it is energetically favorable for the V^{4+}–Mo^{6+} pairs to be bridged by the corner-shared oxygen within an ReO_3-type slab (see Fig. 1), since this results in the largest $V^{4+}(d)$–$O(p\pi)$–

TABLE IV

LIGAND-FIELD PARAMETERS FOR $(Mo_xV_{1-x})_2O_5$

x	k^a	λ^a (eV)	Δ^a (eV)
0.10	1.0	0.010	0.021
0.25	0.8	0.014	0.010
0.28	0.8	0.016	0.010

[a] The errors in k, λ, and Δ are 0.1, 0.002 eV, and 0.003 eV, respectively.

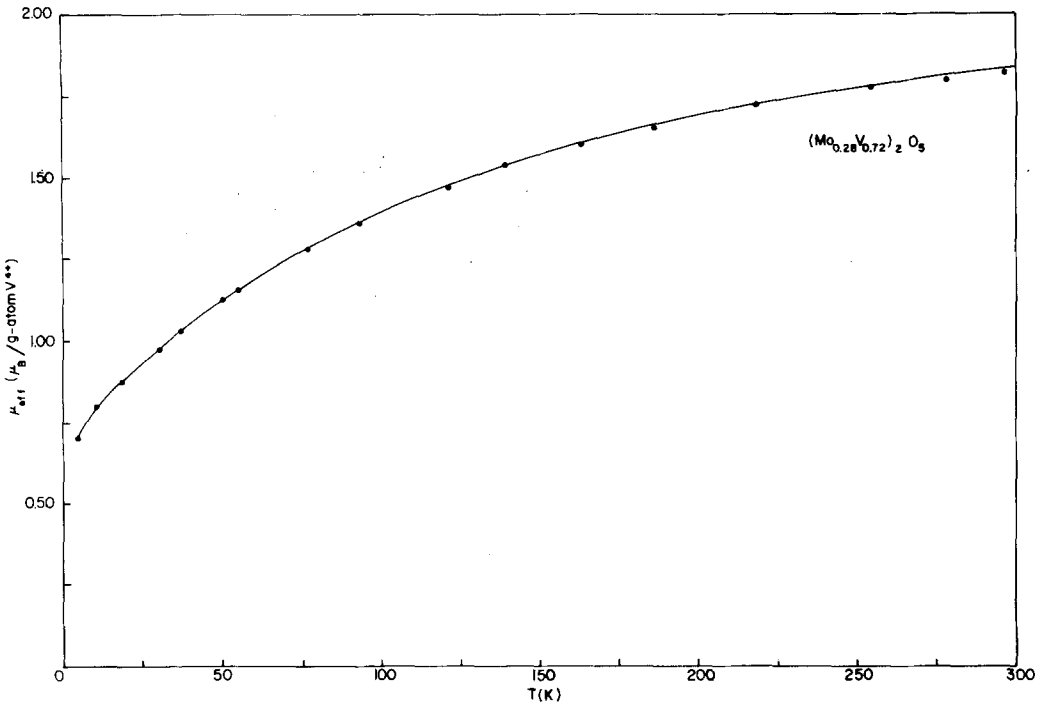

FIG. 3. Comparisons of the experimental (dots) and theoretical (solid curve) moments as a function of temperature for $(Mo_{0.28}V_{0.72})_2O_5$. The solid curve was calculated using $k = 0.8$, $\lambda = 0.016$ ev, and $\Delta = 0.009$ eV.

$Mo^{6+}(d)$ overlap. On this basis it is perhaps possible to understand the difference between the monoclinic and orthorhombic structures shown in Fig. 1. In particular, the pairwise displacement of Mo^{6+} and V^{4+} in opposite directions within an ReO_3-type slab for $x \geq 0.20$ results in maximal 180° $V^{4+}(d)$–$O(p\pi)$–$Mo^{6+}(d)$ overlap within a slab.

However, the displacement of Mo^{6+} and V^{4+} in the same direction for $x \leq 0.20$ will reduce the $V^{4+}(d)$–$O(p\pi)$–$Mo^{6+}(d)$ overlap. Maximal overlap should be preferred, especially at higher Mo concentrations, and experimentally it appears that the pairwise displacement of V^{4+} and Mo^{6+} in opposite directions becomes favored for $x > 0.20$. The structural study of $(Mo_{0.28}V_{0.72})_2O_5$ (*9*) indicates that these pairs should be located randomly within the ReO_3-type slabs. Furthermore, the decrease in k in going from $x = 0.1$ to $x = 0.25$ and 0.28 correlates with the corresponding increase in $V^{4+}(d)$–$O(p\pi)$–$Mo^{6+}(d)$ overlap.

As found in II, the spin–orbit coupling constants are considerably lower than the free-ion value (0.31 eV) and increase with x. In analogy to $VO(H_2O)_5^{2+}$ (*14*), the reduced λ's probably result from the lower effective nuclear charge of vanadium caused by covalent V^{4+}–O bonding. The increase in λ with x suggests a corresponding increase in the effective nuclear charge of vanadium, which could result from the removal of V^{4+} electron density by Mo^{6+}.

The axial distortion can be interpreted in terms of the metal–oxygen distances in Table I. As indicated in II, the small positive Δ's, indicating a slightly compressed C_{4v} symmetry, probably result from the near compensation of the axial compression due

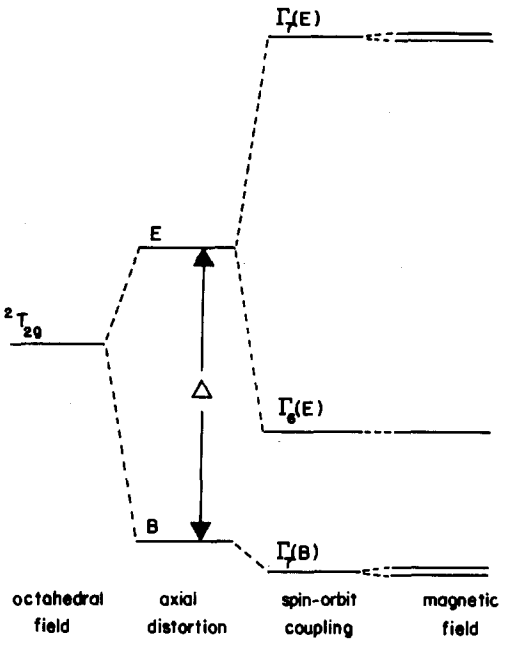

FIG. 4. Energy-level diagram for $(Mo_{0.28}V_{0.72})_2O_5$ showing the effects of axial distortion, spin–orbit coupling, and magnetic field on the $^2T_{2g}$ ground term of the octahedral field.

to the shortest V^{4+}–O bond by the axial expansion resulting from the opposite, longest V^{4+}–O bond. The abrupt decrease in Δ in going from $x = 0.1$ to $x = 0.25$ and 0.28 reflects the more nearly octahedral oxygen arrangement in the monoclinic phase. Specifically, the decrease in Δ follows from the increase in the shortest V^{4+}–O distance (0.074 Å) and the decrease in the longest V^{4+}–O distance (0.241 Å) upon transforming to the monoclinic phase.

Electron Paramagnetic Resonance

Typical EPR spectra of $(Mo_{0.10}V_{0.90})_2O_5$ and $(Mo_{0.25}V_{0.75})_2O_5$ are shown in Figs. 5 and 6. The spectra in the monoclinic phase consisted of a single asymmetric line having $g = 1.96$, which is characteristic of V^{4+}. Better resolution of the asymmetric line is obtained in the orthorhombic phase, and the EPR spectra in this phase could be fitted to Eq. (3) in I. The best least-squares fit of the theoretical spectrum to the experimental one at 50°K is shown in Fig. 5, and the EPR parameters derived from this spectrum are $g_\parallel = 1.908$, $g_\perp = 1.991$, and $\Delta H_{1/2} = 81$ G, where $g_\parallel$ and $g_\perp$ are the g-values parallel and perpendicular to the shortest V^{4+}–O bond, respectively, and $\Delta H_{1/2}$ is the full width at half-maximum absorption. $g_\parallel$ and $g_\perp$ are independent of temperature, and the spin susceptibility behaves paramagnetically in the range 10–300°K, which indicates that only the ground V^{4+} level produces the observed resonance. In the Ballhausen–Gray molecular-orbital scheme for vanadyl complexes (*14*), the above g-values are consistent with a magnetic d_{xy} ground level, which is equivalent to the ground $\Gamma_7(B)$ level found from the magnetic analysis of the last section.

The temperature dependence of the linewidth for $(Mo_{0.10}V_{0.90})_2O_5$ is shown in Fig. 7. The peak-to-peak linewidth, $\Delta H_{p\text{-}p}$, and $\Delta H_{1/2}$ exhibit a similar temperature dependence, so that the temperature dependence of the linewidth can be determined by simply measuring $\Delta H_{p\text{-}p}$. The linewidth decreases with temperature up to about 40°K, has a minimum in the range 40–80°K, and then

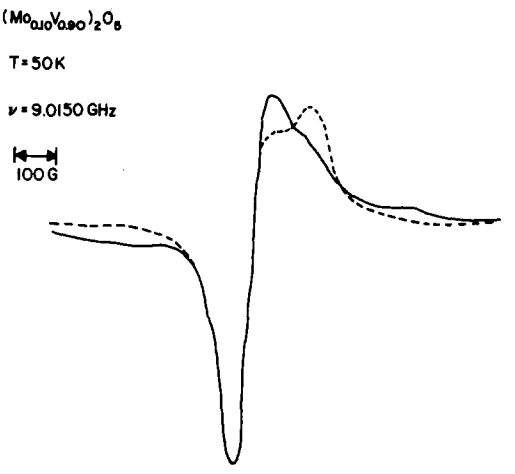

FIG. 5. EPR spectrum of $(Mo_{0.10}V_{0.90})_2O_5$. The broken line was computed from Eq. (3) in I using the parameters $g_\parallel = 1.908$, $g_\perp = 1.991$, and $\Delta H_{1/2} = 81$ G.

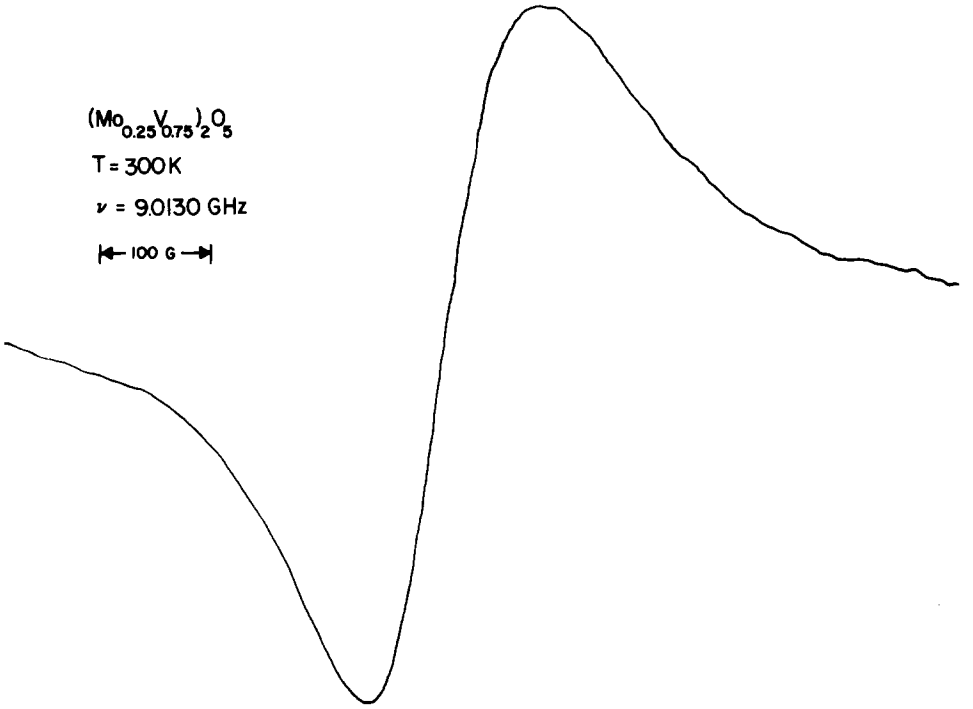

FIG. 6. EPR spectrum of $(Mo_{0.25}V_{0.75})_2O_5$.

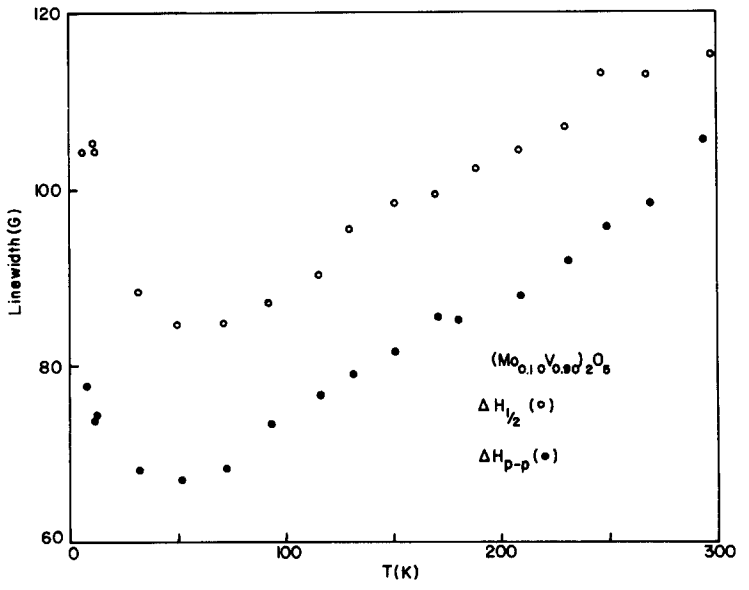

FIG. 7. Temperature dependence of the peak-to-peak linewidth ΔH_{p-p}, and the full width at half-maximum absorption $\Delta H_{1/2}$, for $(Mo_{0.10}V_{0.90})_2O_5$.

increases with temperature above about 80°K. The qualitative interpretation of this behavior is similar to that given in II, with the exception that electronic hopping at low temperatures is unlikely due to the high activation energy. Hence, the decrease in linewidth at low temperatures probably results from occupation of the weakly magnetic, intermediate $\Gamma_6(E)$ level, the minimum at intermediate temperatures may be associated with the nearly equal population of the $\Gamma_6(E)$ and the ground magnetic $\Gamma_7(B)$ levels, and the increase in linewidth at higher temperatures probably reflects occupation of the highest, magnetic $\Gamma_7(E)$ level.

The linewidth vs temperature plots for $(Mo_{0.25}V_{0.75})_2O_5$ and $(Mo_{0.28}V_{0.72})_2O_5$ are shown in Fig. 8 and, as for $(Mo_{0.10}V_{0.90})_2O_5$, can be interpreted using the energy-level diagram derived from the susceptibility studies. In particular, the absence of line broadening as the temperature is lowered follows from the fact that the separation between the $\Gamma_7(B)$ and $\Gamma_6(E)$ levels at these compositions is only one-third the separation at $x = 0.10$, so that the onset of broadening should occur below about 10°K, which is our lowest attainable temperature. The good agreement between the susceptibility and EPR studies in $(Mo_xV_{1-x})_2O_5$ lends strong support to the magnetic analysis of the last section.

Infrared Spectra

The ir spectra in $(Mo_xV_{1-x})_2O_5$ for $x = 0$, 0.1, 0.25, and 0.28 at 300°K are shown in Fig. 9, and the band maxima are given in Table V. The ir spectra and band maxima are in good agreement with a previous study of the V_2O_5–MoO_3 system (*7*). The narrow, high-frequency bands near 1000 cm^{-1} are characteristic of the stretching vibration of the multiple *M*–O bond (*15*), and the broad peaks near 800 cm^{-1} are possibly due to the vibration of polymeric chains *M*–O–*M*–O in which oxygen atoms are common corners of the MO_6 octahedra (*16*). As x is increased from 0 to 0.28 there is a shift in the high-frequency band from 1025 to 1015 cm^{-1},

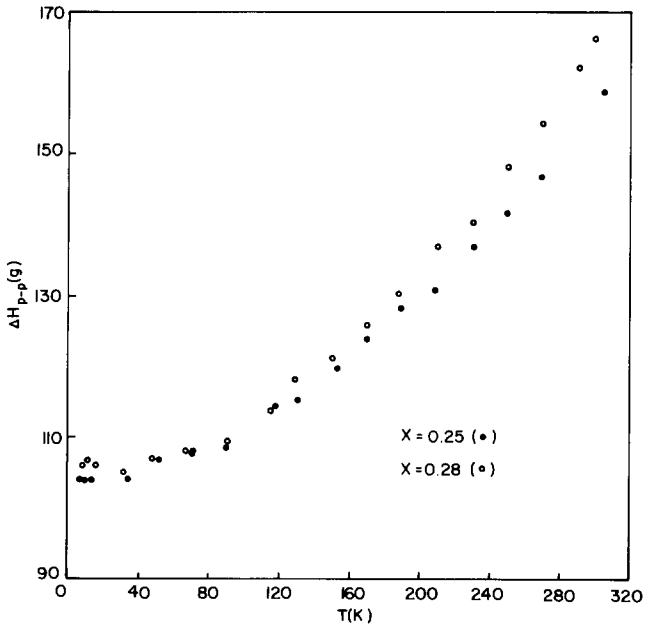

FIG. 8. ΔH_{p-p} vs temperature for $(Mo_{0.25}V_{0.75})_2O_5$ and $(Mo_{0.28}V_{0.72})_2O_5$.

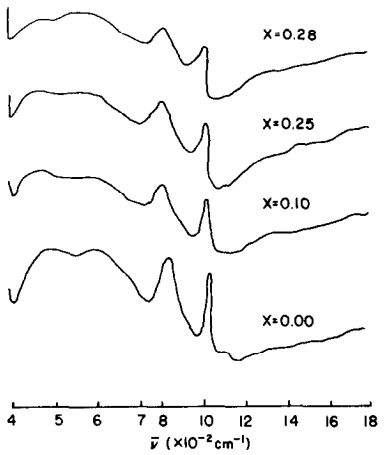

FIG. 9. Infrared spectra of $(Mo_xV_{1-x})_2O_5$ at 300°K.

which suggests a weakening of the shortest M–O bond with increasing Mo content. This is consistent with the increase of 0.074 Å in the shortest M–O distance in going from $x = 0$ to $x = 0.28$ and also with the removal of electron density by Mo^{6+}, as indicated previously by the increase in spin–orbit coupling constant with x. At the molecular level, it is reasonable that the stronger V^{4+}–O–Mo^{6+} interaction in the monoclinic phase will tend to reduce the M–O_1 bonding and hence increase the M–O_1 distance.

Optical Spectra

The optical absorption spectrum of $(Mo_{0.25}V_{0.75})_2O_5$ at 77°K is shown in Fig. 10, and the band maxima are given in Table VI.

TABLE V

INFRARED BAND MAXIMA FOR $(Mo_xV_{1-x})_2O_5$

	Band (cm^{-1})				
x	1	2	3	4	5
0.00	480	600	825	1025	1115
0.10	475	590	820	1025	1115
0.25	475	580	810	1015	1115
0.28	470	575	810	1015	1115

The optical spectrum of $(Mo_{0.28}V_{0.72})_2O_5$ is nearly identical to that in Fig. 10. As discussed in II, the orgin of the individual bands in Fig. 10 is probably vibronic or electronic. The envelope of these bands defines two main ligand-field bands near 10,000 and 15,000 cm^{-1}, which have been designated bands I and II, respectively, in II. As argued in II, the energy of band I should equal 10 Dq. The bands lying above 29,000 cm^{-1} are probably charge-transfer bands. Unfortunately, the two main bands for $x = 0.1$ are too broad to define their positions. However, an optical experiment on a lightly doped sample having $x = 0.01$ at 300°K revealed that band I had shifted to about 8000 cm^{-1}, which indicates a reduction in the octahedral component of the ligand field. This is expected on the basis of the metal–oxygen distances in Table I, since the increase in M–O_1 and decrease in M–O_6 distances as x is increased from 0 to 0.28 should increase the octahedral ligand field at V^{4+}, which is supported by the reduced axial distortion in the monoclinic phase deduced from the susceptibility studies.

Conclusions

The results of this study indicate that the paramagnetic centers in the orthorhombic and monoclinic phases of $(Mo_xV_{1-x})_2O_5$ are deep-donor V^{4+}–O–Mo^{6+} pairs. In the monoclinic phase the oxygen symmetry is more nearly octahedral and the M–O_1 bond is weaker than in the orthorhombic phase.

We have observed that, like V_2O_5, $(Mo_xV_{1-x})_2O_5$ cleaves preferentially perpendicular to the b axis, which exposes the vanadyl oxygen (O_1) on the surface. The weaker V^{4+}–O_1 bond in the monoclinic phase may have some catalytic significance, since vanadyl oxygen plays a special role in the catalytic activity of several molybdates (*17*). In particular, a weaker V^{4+}–O bond would facilitate oxygen release and binding,

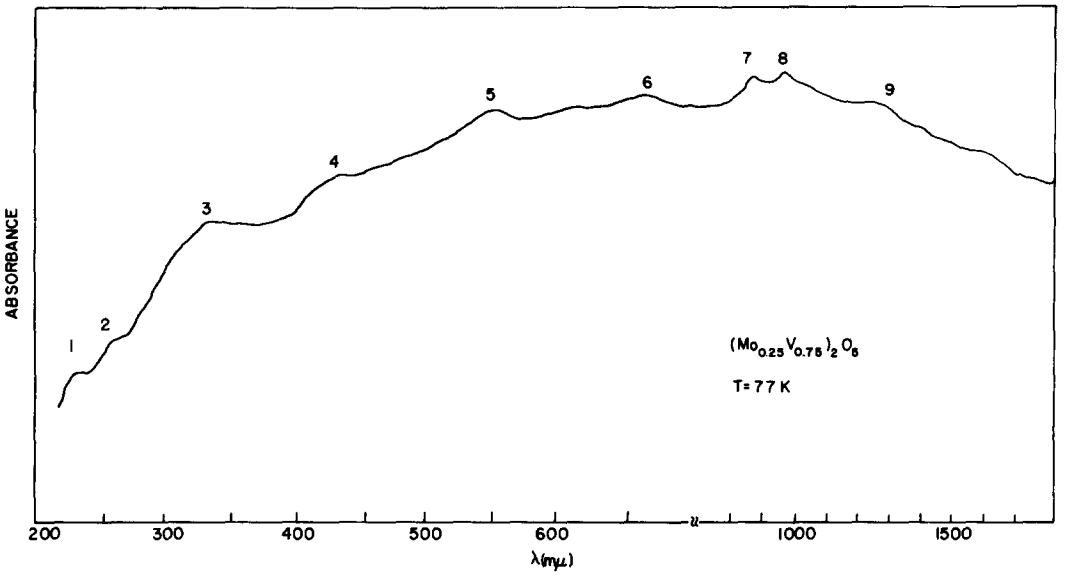

FIG. 10. Optical absorption spectrum of $(Mo_{0.25}V_{0.75})_2O_5$ at 77°K.

which is considered to be an essential function of these catalysts. Hence it is somewhat surprising that the maximum catalytic activity occurs in the range 25–28 mole% MoO_3 (where $x \sim 0.14$), since this compositional range does not correspond to the weakest V^{4+}–O bond.

TABLE VI
OPTICAL BAND MAXIMA FOR $(Mo_{0.25}V_{0.75})_2O_5$

Band	Position (cm^{-1})
1	43,500
2	38,500
3	29,200
4	23,500
5	18,200
6	15,400
7	11,700
8	10.200
9	8,000

References

1. R. H. MUNCH AND E. D. PIERRON, *J. Catal.* **3**, 406 (1964).
2. V. B. KAZANSKII, Z. I. EZHKOVA, A. G. LYUBARSKII, V. V. VOEVODSKII AND I. I. IOFFE, *Kinet. Katal.* **2**, 862 (1961).
3. Z. I. EZHKOVA, I. I. IOFFE, V. B. KAZANSKII, A. V. KRYLOVA, A. G. LYUBARSKII, AND L. Y. MARGOLIS, *Kinet. Katal.* **5**, 861 (1964).
4. K. TARAMA, S. TERANISHI, S. YOSHIDA, AND N. TAMURA, *in* "Proceedings of the Third International Congress on Catalysis," p. 282, North-Holland, Amsterdam (1965).
5. A. SPINZI AND I. V. NICOLESCU, *Rev. Roum. Chim.* **14**, 903 (1969).
6. A. BIELANSKI, K. DYREK, I. KRACIK, AND E. WENDA, *Bull. Acad. Polon. Sci. Ser. Sci. chim.* **19**, 513 (1971).
7. A. BIELANSKI, K. DYREK, AND A. KOZLOWSKA-ROG, *Bull. Acad. Polon. Sci. Ser. Sci. chim.* **20**, 1055 (1972).
8. A. BIELANSKI, R. DZIEMBAJ, K. DYREC, AND E. WENDA, *Bulg. Acad. Sci.* **6**, 531 (1973).
9. L. KILBORG, *Acta. Chem. Scand.* **21**, 2495 (1967).
10. H. G. BACHMANN, F. R. AMED, AND W. J. BARNES, *Acta Chem. Scand.* **4**, 1119 (1950).
11. A. MAGNELI AND B. BLOMBERG, *Acta Chem. Scand.* **5**, 585 (1951).
12. A. CASALOT AND P. HAGENMULLER, *J. Phys. Chem. Solids* **30**, 1341 (1969).
13. J. GALY, J. DARRIET, A. CASALOT, AND J. B. GOODENOUGH, *J. Solid State Chem.* **1**, 339 (1970).
14. C. J. BALLHAUSEN AND H. B. GRAY, *Inorg Chem.* **1**, 111 (1962).

15. J. SELBIN, *Chem. Rev.* **65**, 153 (1965).
16. E. G. BARRACLOUGH, J. LEWIS, AND R. S. NYHOLM, *J. Chem. Soc. London*, 3552 (1959).
17. F. TRIFFIRO, P. CENTOLA, I. PASQUON, AND P. JIRU, 4th International Congress on Catalysis, Moscow, Paper No. 18 (1968).